Preprints of the 19th World Congress
The International Federation of Automatic Control
Cape Town, South Africa. August 24-29, 2014

Slip-Constrained Model Predictive Control Allocation for an All-Wheel Driven Electric Vehicle

T. Bächle * **K. Graichen** * **M. Buchholz** * **K. Dietmayer** *

* *Institute of Measurement, Control and Microtechnology, University of Ulm, Germany (e-mail: {thomas.baechle,knut.graichen, michael.buchholz,klaus.dietmayer}@ uni-ulm.de)*

Abstract: This contribution describes a real-time model predictive control allocation algorithm for over-actuated electric vehicles with individually driven wheels. The proposed method allows to exploit the inherent redundancy present in these systems to optimally allocate yaw moment and longitudinal force while considering actuator dynamics and complying with rate and wheel slip constraints. A linear formulation of the underlying model with varying parameters allows to take changing driving situations into account while guaranteeing fast computation times. The algorithm is tested and validated on a comprehensive vehicle model.

Keywords: Nonlinear and optimal automotive control; Vehicle dynamic systems.

1. INTRODUCTION

In recent years, a trend towards partially or completely electrified drivetrains in production vehicles became apparent. Apart from the obvious advantages regarding energy efficiency, several of those topologies offer additional degrees of freedom to vehicle control strategies. In particular, electric vehicles equipped with two or four wheel-independent drives can not only provide longitudinal force for driving and recuperation purposes, but also actively influence yaw dynamics.

To this end, hierarchical approaches have shown to be beneficial in regard to modularization and reduced complexity. Generally, a high-level controller is used to fulfill control objectives like improved yaw response or a specific desired over- or understeering behavior of the vehicle. Usually, the output of this controller is a moment to be applied to the yaw axis of the vehicle. The main objective of this contribution is a real-time model predictive control allocation strategy to provide this additional yaw moment as well as the longitudinal force requested by the driver. This is done utilizing the available motors optimally while accounting for actuator and wheel slip dynamics as well as for physical limits of the drivetrain and the wheel-ground contact.

The subject of resolving the redundancy of over-actuated systems has been an active field of research, see e. g. Johansen and Fossen (2013) for a comprehensive overview. In fact, various strategies have been proposed ranging from active-set methods (Schofield and Hagglund, 2008), quadratic programming (Plumlee et al., 2004), nonlinear optimization techniques with focus on feasibility (Knobel et al., 2006), and optimal utilization of adhesion potentials (Orend, 2005). Additionally, actuator dynamics can be considered by model predictive control allocation (MPCA)

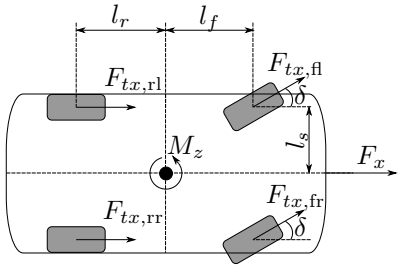

Fig. 1. Geometry of the considered vehicle

as shown by Vermillion et al. (2009) for an automotive thermal management system. However, the application of model predictive control as an on-line optimizing control allocation method taking into account the fast dynamics of wheel slip requires an efficient and real-time capable algorithm. In this contribution, a recently published gradient-based algorithm is utilized to provide optimal solutions to the control allocation problem in real-time.

This paper is organized as follows: Section 2 motivates the considered control allocation problem and also introduces the constraints to adhere to. In Section 3, the proposed control allocation method is introduced and the strategy to include slip constraints is explained. A simulation example in Section 4 demonstrates the performance of the proposed method, while Section 5 gives a short summary.

2. PROBLEM FORMULATION

The considered close-to-production prototype vehicle with the geometry shown in Fig. 1 features four independently controlled motors, where each motor drives one wheel through a fixed transmission unit. The forces, torque and rotational speed of each wheel are given in the wheel's frame of reference. The steering angle δ is directly given by the driver who also commands the longitudinal force F_x using the gas and brake pedals. In addition to the

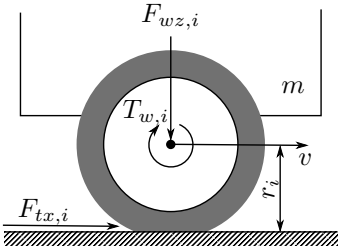

Fig. 2. Quarter vehicle model

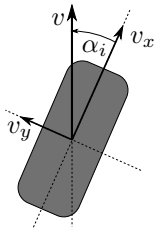

Fig. 3. Tire side slip angle

longitudinal force, the moment about the yaw axis M_z is considered as the second control objective to be allocated by the MPCA scheme using the individual wheel drives. The dependence of these two control objectives on the four longitudinal tire forces $F_{tx,i},\ i \in \{\text{fl,fr,rl,rr}\}$, is given by

$$\begin{aligned} M_z = \boldsymbol{b}_T^{\mathrm{T}} \boldsymbol{F}_{tx} =& (-l_s \cos\delta + l_f \sin\delta) F_{tx,\text{fl}} \\ &+ (l_s \cos\delta + l_f \sin\delta) F_{tx,\text{fr}} \\ &- l_s F_{tx,\text{rl}} + l_s F_{tx,\text{rr}}\,, \end{aligned} \tag{1}$$

$$\begin{aligned} F_x = \boldsymbol{b}_F^{\mathrm{T}} \boldsymbol{F}_{tx} =& \cos\delta (F_{tx,\text{fl}} + F_{tx,\text{fr}}) \\ &+ F_{tx,\text{rl}} + F_{tx,\text{rr}} \end{aligned} \tag{2}$$

with the geometry parameters $\boldsymbol{b}_T$ and $\boldsymbol{b}_F$ and the steering angle δ assumed to be equal between both front wheels. The tire forces themselves are generated by the longitudinal steady-state tire slip κ, which is defined by

$$\kappa = -\frac{v - \omega r}{v} \tag{3}$$

as the normalized difference between the velocity of the tire-road contact patch ωr and the vehicle's longitudinal velocity v as shown in Fig. 2. Furthermore, the relationship between the longitudinal wheel slip κ and the longitudinal tire force F_{tx} is influenced by the normal force on the tire F_{wz}, the tire-road friction coefficient [1] and the tire side slip angle α shown in Fig. 3. Among several existing models describing tire behavior, Pacejka's Magic Formula (Pacejka, 2012) has found wide-spread application due to its high fidelity and is also the base for this contribution. Since

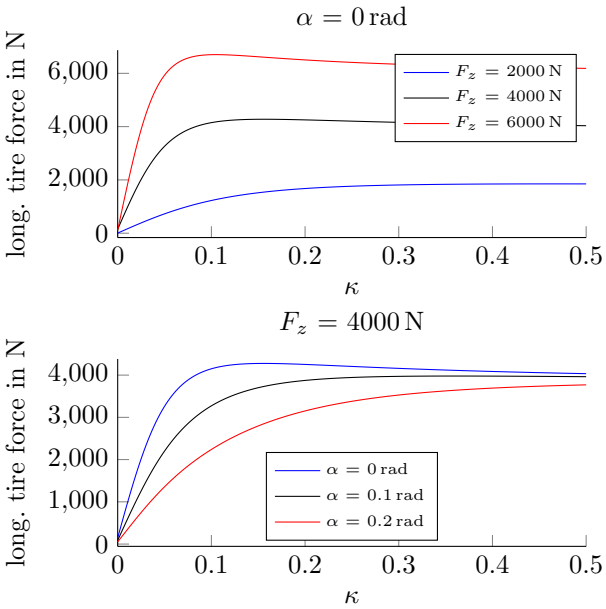

Fig. 4. Longitudinal force over tire slip for several values of F_{wz} and α according to Pacejka's Magic Formula

[1] For this contribution, dry concrete conditions are assumed.

small wheel slip values are generally desired to achieve reduction of drivetrain losses and improved durability of the tires, this contribution intends to constrain wheel slip to values of $|\kappa| < 0.05$. As this constraint can be enforced by the proposed MPCA scheme, a linear approximation

$$\begin{aligned} F_{tx}(\kappa, F_{wz}, \alpha) &\approx c_\kappa(F_{wz}, \alpha)\kappa, \\ c_\kappa(F_{wz}, \alpha) &= \frac{\partial F_{tx}}{\partial \kappa}(0, F_{wz}, \alpha) \end{aligned} \tag{4}$$

can be performed which captures the dependency on normal force and tire side slip angle for small slip values, see Fig. 4. This provides the additional advantage of faster evaluations which is of importance especially for real-time optimization methods, where a large number of evaluations is performed. The prerequisite of small slip values is accounted for by imposing a box constraint

$$\kappa \in \left[-\kappa^+, \kappa^+\right], \quad \kappa^+ > 0\,, \tag{5}$$

on the wheel slips in the MPCA scheme. Considering the system shown in Fig. 2, the dynamics of the wheel slip with respect to the wheel torque $T_{w,i}$ can be described by

$$\dot{\kappa} = -\frac{1}{v}\left(\frac{\kappa - 1}{m} + \frac{r^2}{J}\right) c_\kappa \kappa + \frac{1}{v}\frac{r}{J} T_w \tag{6}$$

using the quarter vehicle mass m and the combined momentum of inertia J given by wheel and motor. Since the dynamics of κ is inversely dependent on the vehicle's velocity v, the slip dynamics becomes increasingly more difficult to control for slower vehicle velocities. Although the first-order approximation given in (6) does not account for relaxation length effects which are more difficult to model and evaluate (see Zegelaar (1998)), this model has proven suitable for wheel slip control in experiments (see Johansen et al. (2003)). Furthermore, the simplification

$$\dot{\kappa} \approx -\frac{1}{v}\left(\frac{r^2}{J} c_\kappa \kappa - \frac{r}{J} T_w\right) \tag{7}$$

can be performed under the assumption $\frac{\kappa - 1}{m} \ll \frac{r^2}{J}$, which holds for large masses of the quarter vehicle and yields a linear system description.

The driving torque T_w for each wheel is provided by an electric motor operated by means of an AC controller in torque-control mode. That introduces an additional first-order linear dynamics of the form

$$\dot{T}_w = -\frac{1}{T_m} T_w + \frac{1}{T_m} T_d \tag{8}$$

with the desired torque T_d as input and the actual torque on the wheel T_w as output, which is assumed equal to T_d in steady-state. Furthermore, the considered motor controllers impose fixed rate limits

$$\left|\dot{T}_w\right| \leq \dot{T}_w^+, \quad \dot{T}_w^+ > 0 \tag{9}$$

on the generated torques. This can be modeled by augmenting (8) with an additional upstream integrator with a limit imposed on its input according to (9).

The combination of (7), (8) and the aforementioned integrator yields the linear model of the quarter vehicle wheel slip dynamics shown in Fig. 5 with one constrained input and a constrained final state. Accordingly, the model equations are given by

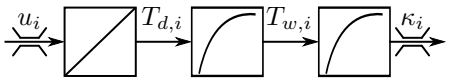

Fig. 5. Overview of resulting wheel slip model

$$\dot{\boldsymbol{x}}_i = \boldsymbol{f}_i(\boldsymbol{x}_i, u_i) = \begin{bmatrix} -\frac{1}{v}\left(\frac{r_i^2}{J_i} c_{\kappa,i} x_{i,1} - \frac{r_i}{J_i} x_{i,2}\right) \\ -\frac{1}{T_m} x_{i,2} + \frac{1}{T_m} x_{i,3} \\ u_i \end{bmatrix}, \quad (10)$$
$$u_i \in [-\dot{T}_{d,i}^+, \dot{T}_{d,i}^+],\ x_{i,1} \in \left[-\kappa^+, \kappa^+\right],$$

with the state vector $\boldsymbol{x}_i = [\kappa_i,\ T_{w,i},\ T_{d,i}]^{\mathrm{T}}$. Combining the four independent quarter vehicle models yields the overall dynamics

$$\dot{\boldsymbol{x}} = \boldsymbol{f}(\boldsymbol{x}, \boldsymbol{u}) = \begin{bmatrix} \boldsymbol{f}_{\mathrm{fl}} & (\boldsymbol{x}_{\mathrm{fl}}, u_{\mathrm{fl}}) \\ \boldsymbol{f}_{\mathrm{fr}} & (\boldsymbol{x}_{\mathrm{fr}}, u_{\mathrm{fr}}) \\ \boldsymbol{f}_{\mathrm{rl}} & (\boldsymbol{x}_{\mathrm{rl}}, u_{\mathrm{rl}}) \\ \boldsymbol{f}_{\mathrm{rr}} & (\boldsymbol{x}_{\mathrm{rr}}, u_{\mathrm{rr}}) \end{bmatrix}, \ \boldsymbol{x} = \begin{bmatrix} \boldsymbol{x}_{\mathrm{fl}} \\ \boldsymbol{x}_{\mathrm{fr}} \\ \boldsymbol{x}_{\mathrm{rl}} \\ \boldsymbol{x}_{\mathrm{rr}} \end{bmatrix}, \ \boldsymbol{u} = \begin{bmatrix} u_{\mathrm{fl}} \\ u_{\mathrm{fr}} \\ u_{\mathrm{rl}} \\ u_{\mathrm{rr}} \end{bmatrix}, \quad (11)$$

which is pivotally defined in its behavior by the vehicle velocity v, the steering angle δ, and the longitudinal tire stiffnesses $c_{\kappa,i}$, which vary during driving according to the maneuvers performed (see (4)). Since the dynamics of these variable parameters are generally governed by the large mass and moment of momentum of the vehicle, they are assumed to be fixed in each sampling step of the MPCA for the duration of the prediction horizon. However, they are updated in each sampling step to account for changing driving conditions.

3. CONTROL ALLOCATION

An MPC scheme is used to optimally allocate wheel torques. In order to improve the convergence behavior of the resulting MPCA scheme, the process of control allocation is subdivided into two stages.

3.1 Static Preallocation

The first stage creates a distribution of the wheel torques and slips solely based on geometrical considerations, determining preallocated values for the torque distribution

$$\hat{\boldsymbol{T}}_w = \left(M_z \boldsymbol{b}_T^{\dagger} + F_x \boldsymbol{b}_F^{\dagger}\right) r_0 \quad (12)$$

with the unloaded tire radius r_0, yielding the wheel torques based on pseudo inverses of $\boldsymbol{b}_T$ and $\boldsymbol{b}_F$. Essentially, the highest torque is assigned to the wheel constituting the most effective lever on the center of gravity. Furthermore, the steady-state slip values

$$\hat{\kappa}_i = \frac{\hat{T}_{w,i}}{r_0 c_{\kappa,i}} \quad (13)$$

are calculated in accordance to (10), which combined with (12) provides preallocated values

$$\hat{\boldsymbol{x}} = \left[\hat{\kappa}_{\mathrm{fl}},\ \hat{T}_{w,\mathrm{fl}},\ \hat{T}_{w,\mathrm{fl},\cdots}\right]^{\mathrm{T}} \quad (14)$$

for the entire state vector. These values represent one possible solution to the control allocation problem, but do not necessarily account for any dynamics or constraints.

3.2 Model Predictive Control Allocation (MPCA)

For the second stage, a recently published gradient-based model predictive control algorithm is employed. It relies on the solution of an optimal control problem (OCP) with an additional penalty term to account for the slip constraints.

Model predictive control relies on the solution of an OCP of the form

$$\min \quad J(\boldsymbol{x}_k, \bar{\boldsymbol{u}}) = \int_{t_k}^{t_k+T} l(\bar{\boldsymbol{x}}(t), \bar{\boldsymbol{u}}(t))\,\mathrm{d}t \quad (15)$$

$$\text{s.t.} \quad \dot{\bar{\boldsymbol{x}}}(t) = \boldsymbol{f}(\bar{\boldsymbol{x}}(t), \bar{\boldsymbol{u}}(t))\,, \quad \bar{\boldsymbol{x}}(t_k) = \boldsymbol{x}_k\,, \quad (16)$$

$$u_i(t) \in [-T_{d,i}^+, T_{d,i}^+]\,, \quad i \in \{\mathrm{fl,fr,rl,rr}\}\,, \quad (17)$$

with the positive definite integral cost function $l\colon \mathbb{R}^{12} \times \mathbb{R}^4 \to \mathbb{R}_0^+$ that is minimized over the prediction horizon $[t_k, t_k + T]$ with the horizon length $T > 0$. The dynamics (16) are given by the linear model (11) of the four quarter vehicle models. The current state at time t_k is denoted by $\boldsymbol{x}_k = \boldsymbol{x}(t_k)$, which represents the initial condition for the MPC scheme. The bounds on the controls (17) account for the rate constraints in (10).

In MPC, it is often assumed that the optimal solution of the OCP (15)-(17)

$$\begin{aligned} \bar{\boldsymbol{u}}_k^*(t) &= \bar{\boldsymbol{u}}^*(t; \boldsymbol{x}_k)\,, \\ \bar{\boldsymbol{x}}_k^*(t) &= \bar{\boldsymbol{x}}^*(t; \boldsymbol{x}_k, \bar{\boldsymbol{u}}_k^*)\,, \quad t \in [t_k, t_k + T]\,, \end{aligned} \quad (18)$$

with the optimal cost $J^*(\boldsymbol{x}_k) = J(\boldsymbol{x}_k, \bar{\boldsymbol{u}}_k^*)$ is computed at time t_k and the first part of the control trajectory $\bar{\boldsymbol{u}}_k^*(t)$ is applied as control input

$$\boldsymbol{u}(t) = \bar{\boldsymbol{u}}_k^*(t)\,, \quad t \in [t_k, t_k + \Delta t) \quad (19)$$

for the system. In the next sampling instant $t_{k+1} = t_k + \Delta t$ with the sampling time $\Delta t > 0$, the OCP (15)-(17) is solved again with the system state $\boldsymbol{x}_{k+1}$ as the new initial condition in (16).

The cost functional in (15) is designed to satisfy several demands:

- to account for the preallocated state (14);
- to avoid high utilization of the inputs;
- to deliver the desired torque $M_{z,d}$ about the yaw axis and the longitudinal force $F_{x,d}$ in accordance to (1), (2), and (4);
- to account for the slip constraints in (10).

The slip constraints $x_{i,1}(t) \in [-\kappa^+, \kappa^+]$ are considered as soft constraints within the cost functional (15) and not as hard constraints in order to maintain the solvability of the OCP (15)-(17) if the constraints are violated (e.g. in unexpected driving situations) and to reduce the numerical complexity of the MPC scheme in view of the future automotive implementation. The four design goals are accounted for by the following terms in the integral cost function:

$$\begin{aligned} l(\boldsymbol{x}, \boldsymbol{u}) = &(\boldsymbol{x} - \hat{\boldsymbol{x}})^{\mathsf{T}} \boldsymbol{Q} (\boldsymbol{x} - \hat{\boldsymbol{x}}) + (\boldsymbol{u} - \hat{\boldsymbol{u}})^{\mathsf{T}} \boldsymbol{R} (\boldsymbol{u} - \hat{\boldsymbol{u}}) \\ &+ \gamma_M (M_z - M_{z,d})^2 + \gamma_F (F_x - F_{x,d})^2 \\ &+ \gamma_\kappa \sum\nolimits_{i=1}^{4} \kappa_{\mathrm{pen}}(\kappa_i)\,. \end{aligned} \quad (20)$$

The penalty function κ_{pen} is designed as

$$\kappa_{\mathrm{pen}}(\kappa_i) = \begin{cases} (\kappa_i/\kappa^+ - 1)^4 & \text{if } \kappa_i \geq \kappa^+ \\ (\kappa_i/\kappa^+ + 1)^4 & \text{if } \kappa_i \leq -\kappa^+ \\ 0 & \text{else} \end{cases}. \quad (21)$$

3.3 Real-time optimization algorithm

The efficient numerical solution of the OCP (15)-(17) is of utmost importance in view of the considerable complexity of the problem ($\boldsymbol{x} \in \mathbb{R}^{12}$, $\boldsymbol{u} \in \mathbb{R}^4$) with respect to the anticipated sampling time in the millisecond range and keeping in mind a future automotive implementation with limited hardware resources.

A suitable real-time MPC algorithm to cope with these problems was recently presented (Graichen and Käpernick, 2012). The algorithm uses a tailored gradient method in combination with an adaptive line search strategy. The gradient method thereby takes advantage of the special structure of the optimality conditions that results from the OCP formulation (15)-(17) without terminal constraints.

With the definition of the Hamiltonian

$$H(\boldsymbol{x}, \boldsymbol{\lambda}, \boldsymbol{u}) = l(\boldsymbol{x}, \boldsymbol{u}) + \boldsymbol{\lambda}^{\mathsf{T}} \boldsymbol{f}(\boldsymbol{x}, \boldsymbol{u}) \,, \quad \boldsymbol{\lambda} \in \mathbb{R}^{12} \,, \tag{22}$$

and assuming an initial control trajectory $\bar{\boldsymbol{u}}_k^{(0)}(t)$ and initial state $\bar{\boldsymbol{x}}_k^{(0)}(t)$, $t \in [t_k, t_k + T]$, that satisfies the constraints (17), a gradient iteration j consists of the following steps:

- Forward integration of the system dynamics:

$$\dot{\bar{\boldsymbol{x}}}_k^{(j)}(t) = \boldsymbol{f}\left(\bar{\boldsymbol{x}}_k^{(j)}(t), \bar{\boldsymbol{u}}_k^{(j)}(t)\right) \,, \qquad \bar{\boldsymbol{x}}_k^{(j)}(t_k) = \boldsymbol{x}_k \,. \tag{23}$$

- Backward integration of the adjoint dynamics:

$$\dot{\bar{\boldsymbol{\lambda}}}_k^{(j)}(t) = -H_{\boldsymbol{x}}\left(\bar{\boldsymbol{x}}_k^{(j)}(t), \bar{\boldsymbol{\lambda}}_k^{(j)}(t), \bar{\boldsymbol{u}}_k^{(j)}(t)\right) , \qquad \bar{\boldsymbol{\lambda}}_k^{(j)}(t_k + T) = \boldsymbol{0} \,, \tag{24}$$

  with $H_{\boldsymbol{x}} = \frac{\partial H}{\partial \boldsymbol{x}}$.
- Computation of the search direction:

$$\bar{\boldsymbol{s}}_k^{(j)}(t) = -H_{\boldsymbol{u}}\left(\bar{\boldsymbol{x}}_k^{(j)}(t), \bar{\boldsymbol{\lambda}}_k^{(j)}(t), \bar{\boldsymbol{u}}_k^{(j)}(t)\right) \,, \qquad t \in [t_k, t_k + T] \tag{25}$$

  with $H_{\boldsymbol{u}} = \frac{\partial H}{\partial \boldsymbol{u}}$.
- Step size computation by (approximately) solving:

$$\tilde{\alpha}_k^{(j)} = \arg\min_{\tilde{\alpha} > 0} J\left(\boldsymbol{x}_k, \boldsymbol{\psi}\left(\bar{\boldsymbol{u}}_k^{(j)} + \tilde{\alpha} \bar{\boldsymbol{s}}_k^{(j)}\right)\right) \,, \tag{26}$$

  where $\boldsymbol{\psi} = [\psi_{fl}, \ldots, \psi_{rr}]^{\mathsf{T}}$ is a point-wise in time projection function defined by

$$\psi_i(u_i) = \begin{cases} u_i & \text{if } u_i \in (-\dot{T}_{d,i}^{+}, \dot{T}_{d,i}^{+}) \\ -\dot{T}_{d,i}^{+} & \text{if } u_i \leq -\dot{T}_{d,i}^{+} \\ \dot{T}_{d,i}^{+} & \text{if } u_i \geq \dot{T}_{d,i}^{+} \,. \end{cases} \tag{27}$$

- Control update:

$$\bar{\boldsymbol{u}}_k^{(j+1)}(t) = \boldsymbol{\psi}\left(\bar{\boldsymbol{u}}_k^{(j)}(t) + \tilde{\alpha} \bar{\boldsymbol{s}}_k^{(j)}(t)\right) \,, \qquad t \in [t_k, t_k + T] \,. \tag{28}$$

One gradient step basically consists of two integrations of the adjoint and system dynamics (24) and (23) as well as the solution of the line search problem (26) that basically forms a scalar optimization problem. In the MPC implementation, (26) is approximately solved by using a polynomial fitting with three sample points $\tilde{\alpha}_1 < \tilde{\alpha}_2 < \tilde{\alpha}_3$ that are adapted over the single gradient iterations (Graichen and Käpernick (2012)).

In order to ensure real-time feasibility and a constant computational load in each MPC step, a fixed number N of gradient iterations (i.e. $j = 0, 1, \ldots, N-1$) is used in each MPC step and the first part of the control trajectory $\bar{\boldsymbol{u}}_k^{(N)}(t)$ is applied as control input, i.e.

$$\boldsymbol{u}(t) = \bar{\boldsymbol{u}}_k^{(N)}(t) \,, \quad t \in [t_k, t_k + \Delta t) \,. \tag{29}$$

In the next MPC step $k+1$, $\bar{\boldsymbol{u}}_k^{(N)}(t)$ is recycled to reinitialize the gradient algorithm.

In contrast to the optimal solution (18) and the optimal MPC control (19), this premature stopping criterion will in general result in suboptimal trajectories in the sense that

$$J\left(\boldsymbol{x}_k, \bar{\boldsymbol{u}}_k^{(N)}\right) \geq J^*(\boldsymbol{x}_k) \,. \tag{30}$$

However, incremental improvement as well as asympotic stability of the MPC scheme is nevertheless guaranteed if the number of iterations N is sufficiently large, as shown in Graichen and Kugi (2010); Graichen and Käpernick (2012).

The gradient-based MPC scheme used in this paper is implemented in the software `GRAMPC` (`GRA`dient based `MPC` – [græmp′si:]) that will be made available as open source within the next weeks. `GRAMPC` also includes an interface to MATLAB/SIMULINK with an additional MATLAB GUI in order to provide a convenient and interactive MPC design procedure (Käpernick and Graichen (2014)).

4. RESULTS

The proposed strategy for dynamic control allocation in an experimental vehicle is validated in simulations on a comprehensive nonlinear vehicle model which was developed following Schramm et al. (2010). This vehicle model comprises nine coupled bodies with fourteen degrees of freedom. It accepts front steering angle and individual wheel torques as inputs and is parameterized to represent a medium sized sedan. In contrast to the simplified model used within the MPCA scheme, this model explicitly considers suspension influences regarding load transfer as well as rolling friction and aerodynamic drag. Simulation of the tire behavior is performed according to Pacejka (2012) including relaxation lengths and combined slip conditions. Additionally, the vehicle model provides feedback for the vertical tire loads $F_{wz,i}$, the tire side slip angles α_i, as well as the vehicle speed v. Those variables update the underlying system model (11) within the MPCA scheme.

The drivetrain is modeled in accordance to the motor dynamics (8) and the rate limits (9). Table 1 shows the most important parameters of the simulation setup.

The performance of the MPCA approach will be demonstrated in a substantial longitudinal deceleration scenario and an aggressive lane change maneuver featuring large lateral accelerations. In all cases, the input constraints are set to

$$\dot{T}_{d,i}^{+} = \begin{cases} 800\,\mathrm{N\,m/s}\,, & \text{for} \quad i \in \{\mathrm{fl}, \mathrm{fr}\} \\ 1000\,\mathrm{N\,m/s}\,, & \text{for} \quad i \in \{\mathrm{rl}, \mathrm{rr}\} \end{cases} .$$

These rather restrictive limits are imposed since similar values are implemented by motor controllers considered for the prototype vehicle which is the scope of this contribution. Additionally, in actual applications, a corresponding

Table 1. Parameters of the MPCA scheme and the simulation model

parameter	value
$\hat{\boldsymbol{u}}$	$\left[(0,0,0,0)\,\mathrm{N\,m\,s^{-1}}\right]^{\mathrm{T}}$
$\boldsymbol{Q}$	$\mathrm{diag}\left(1, 100\,\mathrm{N^{-2}\,m^{-2}}, 100\,\mathrm{N^{-2}\,m^{-2}}, \cdots\right)$
$\boldsymbol{R}$	$\mathrm{diag}\,(1,1,1,1)\,\mathrm{s^2\,N^{-2}\,m^{-2}}$
γ_M	$5000\,\mathrm{N^{-2}\,m^{-2}}$
γ_F	$2500\,\mathrm{N^{-2}}$
γ_κ	2.5×10^{12}
T	0.05 s
N_{hor}	26
N	3
Δt	2 ms
T_m	0.1 s
J_{fl}, J_{fr}	$1.6965\,\mathrm{kg\,m^2}$
J_{rl}, J_{rr}	$0.4037\,\mathrm{kg\,m^2}$
r_i	0.307 m
l_f, l_r	1.38 m
l_s	0.7705 m

rate limit may be implemented to prevent damage to the transmission units due to gear lash zone effects. Since the input constraints inherently guarantee that the rate limits are met, the internal state prediction of the desired wheel torques can be used directly as command to the corresponding motor controllers.

4.1 Longitudinal Deceleration

In the first simulation scenario, the driver commands a negative longitudinal force $F_{x,d}$ corresponding to a longitudinal deceleration of about $-5\,\mathrm{m/s^2}$ for a period of 2 s with an initial velocity of 100 km/h. The corresponding trajectories for the cases of disabled slip limit (solid) and an imposed slip limit of $\kappa^+ = 0.025$ (dotted) are shown in Fig. 6. This maneuver gives rise to considerable changes in tire stiffnesses due to load transfer influencing the dynamics (11). The effect of the rate limits are obvious in the slow gradient in the allocated longitudinal force F_x, while the bang-bang-like control action is visible in the trajectory of the input values u_i. In the upper left plot of Fig. 6 the wheel slip values are shown which exhibit undesirably high values on the rear axle for the unconstrained case. In the constrained case, however, the slip value only momentarily overshoots the limit owing to the penalty terms in (20). Despite the active slip constraint on the rear axle, the desired value of F_x is allocated reproducibly by the MPCA scheme, which shifts effort onto the front axle to compensate for the active constraint.

4.2 Lange Change with High Lateral Displacement

For the second example, a reference model approach is used to generate appropriate desired values for the yaw moment $M_{z,d}$. Based on the driver's commands on the steering wheel and the vehicle velocity, a single-track model generates a yaw rate trajectory which is used as a reference to a P-type feedback controller, which determines the desired yaw moment $M_{z,d}$. The single-track reference model is parameterized to correspond to the comprehensive model with three quarters of the yaw axis' moment of inertia, yielding a faster yaw rate response. Since the focus of this contribution is the control allocation scheme, this relatively simple approach was chosen over more sophisticated methods to create desired yaw moments.

Fig. 7 shows the trajectories for this scenario for an aggressive steering action at a velocity of about 70 km/h, during which the steering wheel is operated in a lane-change resembling maneuver featuring higher lateral displacement. As was the case considered in the previous example, the reference yaw moment is tracked accurately and without significant difference between the constrained and unconstrained cases. In this scenario, however, the change in tire stiffnesses is more prominent due to considerable load transfer caused by lateral acceleration as well as the tire side slip angle. In the period from 3.5 s to 4.5 s, the slip constraints of $\kappa^+ = 0.015$ chosen for this example become active. During that time, the steering wheel is turned from one extremal point to the other, decreasing vertical load of the two wheels previously on the outer side of the curve. This necessitates a quick reaction of the MPCA scheme due to the already applied wheel torque and the considerable dynamics of the drivetrain(11). As shown in Fig. 7, the constraints are again met with minimal overshoot.

In light of the velocity-dependent dynamics (11), the sampling time of the MPCA scheme needs to be sufficiently small for the considered speed range. The choice of the sampling time $\Delta t = 2$ ms has proven sufficient for speeds up from 4 m/s. Each sampling step requires a fixed computation time [2] of 150 µs, which is well below the sampling time. Since the scope of this contribution is not yet the direct implementation on board an experimental vehicle, some potential for improved performance remains.

5. CONCLUSION

In this contribution, a strategy to optimally operate overactuated electric vehicles was presented. The corresponding constrained dynamic control allocation problem was solved employing a gradient based MPC scheme. Despite the simplifications performed to achieve real-time capability, the results demonstrate this approach as a very powerful method of resolving the redundancy represented by the considered topology and reproducibly allocating the desired value for yaw moment and longitudinal force while adhering to the constraints on slip values and the rate limits on the wheel torques. Besides the inclusion of online estimations of tire side slip angle and normal load, further work will be focused on energy efficiency and adhering to constraints imposed by the traction battery.

ACKNOWLEDGMENTS

This work is supported by the German "Federal Ministry of Education and Research" (BMBF) within the priority program "ICT2020" under project funding reference number "16N11869".

REFERENCES

Graichen, K. and Käpernick, B. (2012). A real-time gradient method for nonlinear model predictive control. In *Frontiers of Model Predictive Control*, 9–28. InTech.

[2] computed on an Intel i7-2620M at 2.7 GHz

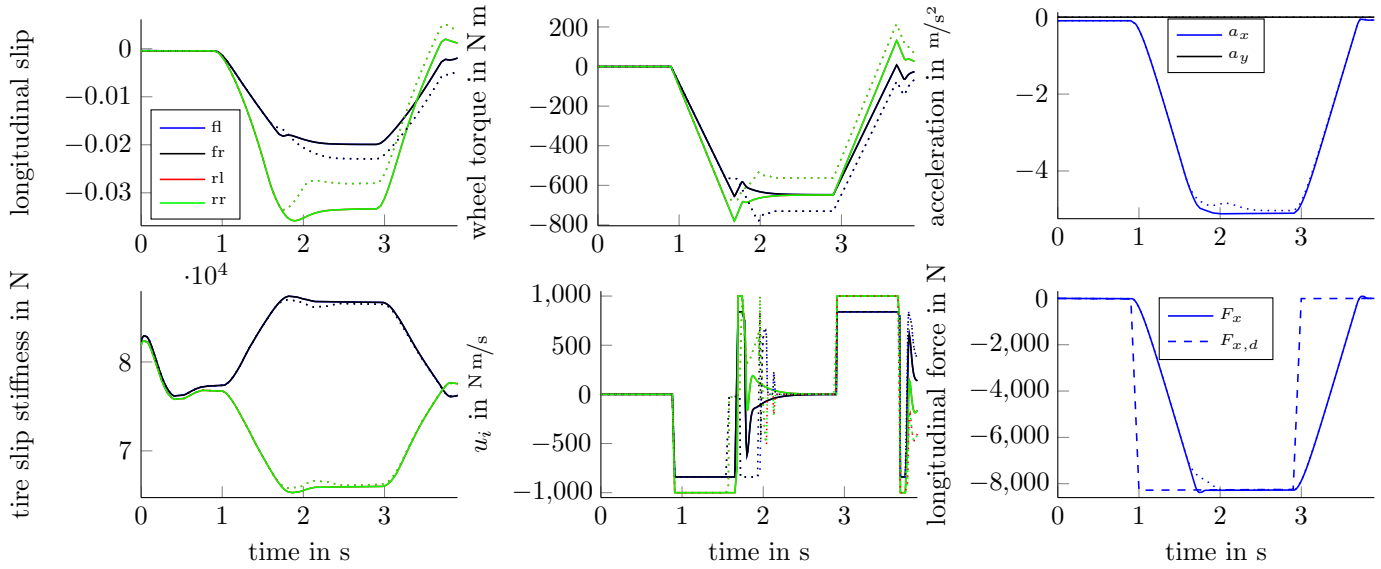

Fig. 6. Unconstrained (solid) and constrained (dotted) trajectories for longitudinal deceleration

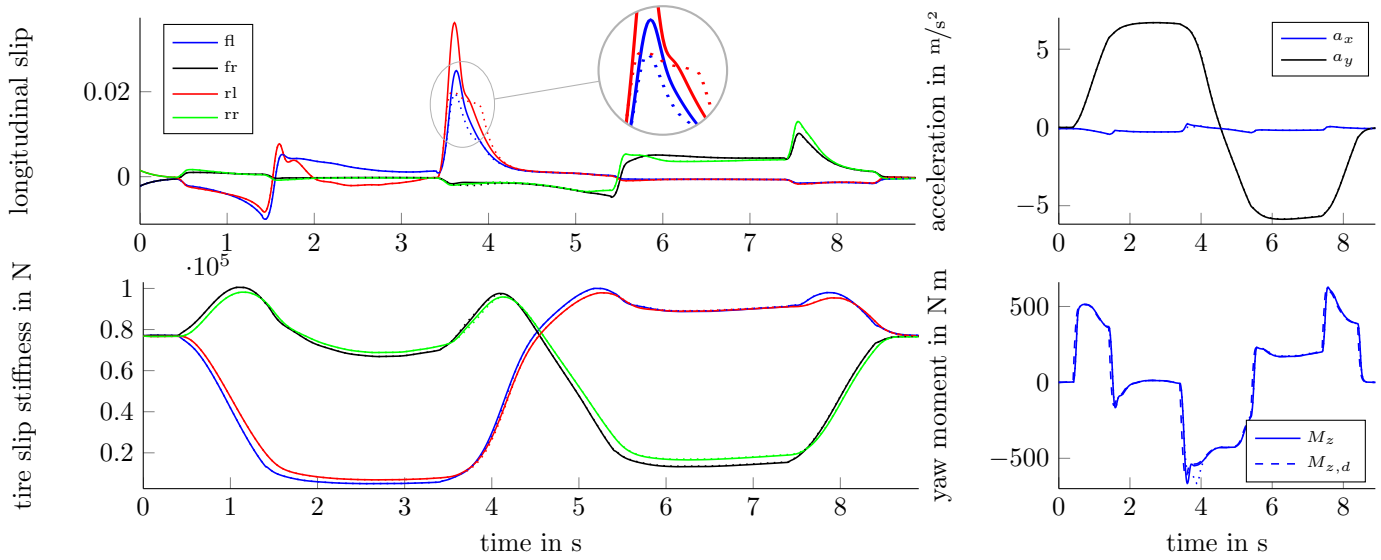

Fig. 7. Unconstrained (solid) and constrained (dotted) trajectories for lane change

Graichen, K. and Kugi, A. (2010). Stability and incremental improvement of suboptimal mpc without terminal constraints. *IEEE Transactions on Automatic Control*, 55(11), 2576–2580.

Johansen, T., Petersen, I., Kalkkuhl, J., and Ludemann, J. (2003). Gain-scheduled wheel slip control in automotive brake systems. *IEEE Transactions on Control Systems Technology*, 11(6), 799–811.

Johansen, T.A. and Fossen, T.I. (2013). Control allocation - a survey. *Automatica*, 49(5), 1087–1103.

Käpernick, B. and Graichen, K. (2014). The gradient based nonlinear model predictive control software GRAMPC. Submitted to 13th European Control Conference (ECC).

Knobel, C., Pruckner, A., and Bunte, T. (2006). Optimized force allocation - a general approach to control and to investigate the motion of over-actuated vehicles. In *Mechatronic Systems*, 366–371.

Orend, R. (2005). Modelling and control of a vehicle with single-wheel chassis actuators. In *Proc. of the 16th IFAC World Congress*, 1900–1905.

Pacejka, H.B. (2012). *Tire and Vehicle Dynamics*. Butterworth-Heinemann, Oxford, 3. edition.

Plumlee, J., Bevly, D., and Hodel, A. (2004). Control of a ground vehicle using quadratic programming based control allocation techniques. In *Proc. of the American Control Conference (ACC)*, 4704–4709.

Schofield, B. and Hagglund, T. (2008). Optimal control allocation in vehicle dynamics control for rollover mitigation. In *Proc. of the American Control Conference (ACC)*, 3231–3236.

Schramm, D., Hiller, M., and Bardini, R. (2010). *Modellbildung und Simulation der Dynamik von Kraftfahrzeugen*. Springer, Berlin.

Vermillion, C., Sun, J., and Butts, K. (2009). Model predictive control allocation - design and experimental results on a thermal management system. In *Proc. of the American Control Conference (ACC)*, 1365–1370.

Zegelaar, P.W.A. (1998). *The dynamic response of tyres to brake torque variations and road unevennesses*. Ph.D. thesis, Delft University of Technology.